Journal of Theoretical Biology 289 (2011) 181–196

Contents lists available at SciVerse ScienceDirect

Journal of Theoretical Biology

journal homepage: www.elsevier.com/locate/yjtbi

The role of seasonality and import in a minimalistic multi-strain dengue model capturing differences between primary and secondary infections: Complex dynamics and its implications for data analysis

Maíra Aguiar [a,b,*], Sebastien Ballesteros [a], Bob W. Kooi [c], Nico Stollenwerk [a]

[a] Centro de Matemática e Aplicações Fundamentais da Universidade de Lisboa, Avenida Prof. Gama Pinto 2, 1649-003 Lisboa, Portugal
[b] Fundação Ezequiel Dias, Serviço de Virologia e Riquetisioses, Laboratório de dengue e febre amarela, Rua Conde Pereira Carneiro 80, 30510-010 Belo Horizonte-MG, Brazil
[c] Vrije Universiteit, Faculty of Earth and Life Sciences, Department of Theoretical Biology, De Boelelaan 1087, NL 1081 HV Amsterdam, The Netherlands

ARTICLE INFO

Article history:
Received 27 February 2011
Received in revised form
25 May 2011
Accepted 30 August 2011
Available online 9 September 2011

Keywords:
Dengue fever
Multi-strain model
Seasonality
Import factor
Predictability

ABSTRACT

In many countries in Asia and South-America dengue fever (DF) and dengue hemorrhagic fever (DHF) has become a substantial public health concern leading to serious social-economic costs. Mathematical models describing the transmission of dengue viruses have focussed on the so-called antibody-dependent enhancement (ADE) effect and temporary cross-immunity trying to explain the irregular behavior of dengue epidemics by analyzing available data. However, no systematic investigation of the possible dynamical structures has been performed so far. Our study focuses on a seasonally forced (non-autonomous) model with temporary cross-immunity and possible secondary infection, motivated by dengue fever epidemiology. The notion of at least two different strains is needed in a minimalistic model to describe differences between primary infections, often asymptomatic, and secondary infection, associated with the severe form of the disease. We extend the previously studied non-seasonal (autonomous) model by adding seasonal forcing, mimicking the vectorial dynamics, and a low import of infected individuals, which is realistic in the dynamics of dengue fever epidemics. A comparative study between three different scenarios (non-seasonal, low seasonal and high seasonal with a low import of infected individuals) is performed. The extended models show complex dynamics and qualitatively a good agreement between empirical DHF monitoring data and the obtained model simulation. We discuss the role of seasonal forcing and the import of infected individuals in such systems, the biological relevance and its implications for the analysis of the available dengue data. At the moment only such minimalistic models have a chance to be qualitatively understood well and eventually tested against existing data. The simplicity of the model (low number of parameters and state variables) offer a promising perspective on parameter values inference from the DHF case notifications.

1. Introduction

Dengue is a viral mosquito-borne infection which in recent years has become a major international public health concern, a leading cause of illness and death in the tropics and subtropics. It is estimated that every year, there are 70–500 million dengue infections, 36 million cases of dengue fever (DF) and 2.1 million cases of dengue hemorrhagic fever (DHF), with more than 20,000 deaths per year (World Health Organization, 2009); Pediatric Dengue Vaccine Initiative. Dengue is caused by four antigenically distinct but closely related viruses, designated by dengue types 1,2,3, and 4, where infection by one serotype confers life-long immunity to only that serotype and a short period of temporary cross-immunity to other serotypes (World Health Organization, 2009; Alcon et al., 2002; Matheus et al., 2005); Lemos, Pers comm.; Diniz, Pers comm.; Halstead, Pers comm.; (Wearing and Rohani, 2006; Halstead, 2004; Dejnirattisai et al., 2010). Two variants of the disease exist: dengue fever (DF), a non-fatal form of illness, and dengue hemorrhagic fever (DHF), which may evolve toward a severe form known as dengue shock syndrome (DSS). Epidemiological studies support the association of DHF with secondary dengue infection (Guzmán et al., 2000; David, 2000; Halstead, 1982, 2003; Nisalak et al., 2003), and there is good evidence that sequential infection increases the risk of developing DHF, due to a process described as antibody-dependent enhancement

* Corresponding author at: Centro de Matemática e Aplicações Fundamentais da, Universidade de Lisboa, Avenida Prof. Gama Pinto 2, 1649-003 Lisboa, Portugal.
E-mail addresses: maira@ptmat.fc.ul.pt, mairaaguiar@yahoo.com.br (M. Aguiar), sebastien.ballesteros@gmail.com (S. Ballesteros), kooi@falw.vu.nl (B.W. Kooi), nico@ptmat.fc.ul.pt (N. Stollenwerk).

0022-5193/$ - see front matter © 2011 Elsevier Ltd. All rights reserved.
doi:10.1016/j.jtbi.2011.08.043

(ADE) (World Health Organization, 2009; Halstead, 2004; Dejnirattisai et al., 2010). The risk for DHF with a third or fourth dengue infection relative to a first or second exposure is not known. An analysis of a database of admitted cases to the Queen Sirikit National Institute of Child Health and Kamphaeng Phet Provincial Hospital with suspected dengue illness revealed that the number of dengue admissions caused by a third or fourth dengue virus infection was extremely low and once admitted, the risk for DHF relative to DF was not different for those experiencing third or fourth dengue virus infections over those experiencing a second dengue virus infection (Endy et al., 2002; Gibbons et al., 2007; Halstead, 2008). It is suggested that the majority of secondary dengue infections occur at a spacing of more than 6 months(Lemos, Pers comm.; Diniz, Pers comm.; Halstead, Pers comm.), and from cohort studies and prospective seroepidemiological studies of defined populations, the hospitalization rates for individuals experiencing secondary dengue infections are in the range of 2–3% of all infected individuals (Halstead, 2003; Rothman, 2004). There is no specific treatment for dengue, and a vaccine is not yet available. So far, prevention of exposure and vector control remain the only alternatives to prevent dengue transmission.

Mathematical models describing the transmission of dengue viruses appeared in the literature as early as 1970 (Fischer and Halstead, 1970). More recently, mathematical models describing the transmission of dengue viruses have focussed on the ADE effect and temporary cross-immunity trying to explain the irregular behavior of dengue epidemics. In the literature the multi-strain interaction leading to deterministic chaos via ADE has been described previously, e.g. Ferguson et al. (1999), Schwartz et al. (2005), and Billings et al. (2007) but neglecting temporary cross-immunity. Consideration of temporary cross-immunity is rather complicated and up to now not in detail analyzed. Models formulated in Wearing and Rohani (2006), Nagao and Koelle (2008), Recker et al. (2009) and Wikramaratna et al. (2010), did not investigate closer the possible dynamical structures. In Aguiar and Stollenwerk (2007), Aguiar et al. (2008), Aguiar et al. (2009) by including temporary cross-immunity into dengue models with ADE, a rich dynamic structure including deterministic chaos was found in wider and more biologically realistic parameter regions. However, in order to be able to reproduce the yearly cycle in dengue incidence seasonal forcing and a low import of infected have to be included in the models.

In addition to *ab initio* simulation techniques to solve the mathematical model numerically, we use bifurcation analyses to study the dependence of the dynamics on parameter values. This separates the parameter space in regions with qualitatively different long-term dynamics: steady-state solution (equilibrium), periodic solution (limit cycle) and non-periodic solution (aperiodic or chaotic attractors). For non-periodic solutions the dynamics is classified further based on Lyapunov exponents. In the case of sinusoidal forcing the non-autonomous system is, for analysis purposes, replaced by an equivalent autonomous system whereby the original model is augmented with the so-called Hopf oscillator producing the sinusoidal forcing.

In this paper, we investigate the extended multi-strain model with temporary cross-immunity and possible secondary infection, motivated by dengue fever epidemiology presented first in Aguiar and Stollenwerk (2007) and Aguiar et al. (2008, 2009). We add seasonal forcing into the previous multi-strain dengue model, mimicking the vectorial dynamics, and a low import of infected individuals, which is realistic in the dynamics of dengue fever epidemics. The complete analysis of the extended models shows complex dynamics and qualitatively a very good result when comparing empirical DHF data and model simulation. The effects of the vector dynamics are only taken into account by the force of infection parameters in the SIR-type model, but not modelling this mechanisms explicitly (see also Wearing and Rohani, 2006). Since vector models without multi-strain aspects only shows stationary dynamics (Esteva and Vargas, 1998, 2000) and seasonally forced SIR systems can show already deterministic chaos (Stone et al., 2007), the presented model is minimalistic in the sense that it can capture the essential differences of primary versus secondary infection under periodic forcing but is not too high dimensional so that future parameter estimation can still attempt to estimate all initial conditions as well as the few model parameters.

2. The seasonal multi-strain epidemic model

The seasonal multi-strain model is represented in Fig. 1 by using a state flow diagram, dividing the population into 10 classes: susceptible to both strains, 1 and 2 (S), primarily infected with strain one (I_1) or strain two (I_2), recovered from the first infection with strain one (R_1) or strain two (R_2), susceptible with a previous infection with strain one (S_1) or strain two (S_2), secondarily infected with strain one when the first infection was caused by strain two (I_{21}) or for second time infected with strain two when the first infection was caused by strain one (I_{12}). Notice that infection by one serotype confers life-long immunity to that serotype. Then the recovered individuals from the secondary infection (R). To give more reality to the dynamics of the disease, we also add a low import factor of infected individuals into the system.

The complete system of ordinary differential equations for the seasonal multi-strain epidemiological model is shown in system (1), and the dynamics are described as follows. Susceptibles to both strains can get the first infection with strain one or strain two with force of infection $\beta I/N$ when the infection is acquired via an individual in his first infection or $\phi\beta I/N$ when the infection is acquired via an individual in his second infection (for more information on the parametrization of ADE and secondary dengue infection by ϕ, see Ferguson et al. (1999) and Aguiar et al. (2008). They recover from the first infection with a recovery rate γ, conferring full and life-long immunity against the strain that they

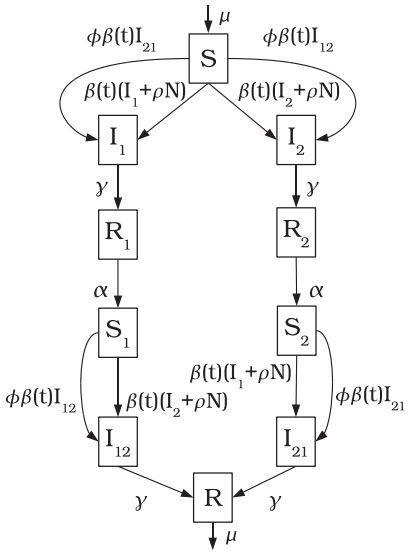

Fig. 1. The state flow diagram for the seasonal two-strain model. The boxes represent the disease related stages and the arrows indicate the transition rates. The transition rate μ coming out of the class R represents the death rates of all classes, $S,I_1,I_2,R_1,R_2,S_1,S_2,I_{12},I_{21},R$, getting into the class S as a birth rate.

were exposed to, and also a short period of temporary cross-immunity α against the other strain, becoming susceptible to a second infection with a different strain. The susceptible with a previous infection gets the secondary infection with force of infection $\beta I/N$ or $\phi\beta I/N$ depending on whom (individual on his primary or secondary infection) is transmitting the infection. Then, with recovery rate γ, the individuals recover and become immune against all strains. We assume no epidemiological asymmetry between strains ($\beta_1=\beta_2=\beta$, $\phi_1=\phi_2=\phi$), i.e. infections with strain one or strain two contribute in the same way to the force of infection. Here, the only relevant difference concerning disease transmissibility is that the force of infection varies accordingly to the number of previous infections the hosts have experienced. In a primary infection the individuals transmit the disease with a force of infection $\beta I/N$ whereas in a secondary infection the transmission is given with a force of infection $\phi\beta I/N$ where ϕ can be larger or smaller than unit, i.e. increasing or decreasing the transmission rate:

$$\dot{S}=-\frac{\beta(t)}{N}S(I_1+\rho\cdot N+\phi I_{21})-\frac{\beta(t)}{N}S(I_2+\rho\cdot N+\phi I_{12})+\mu(N-S)$$

$$\dot{I}_1=\frac{\beta(t)}{N}S(I_1+\rho\cdot N+\phi I_{21})-(\gamma+\mu)I_1$$

$$\dot{I}_2=\frac{\beta(t)}{N}S(I_2+\rho\cdot N+\phi I_{12})-(\gamma+\mu)I_2$$

$$\dot{R}_1=\gamma I_1-(\alpha+\mu)R_1$$

$$\dot{R}_2=\gamma I_2-(\alpha+\mu)R_2$$

$$\dot{S}_1=-\frac{\beta(t)}{N}S_1(I_2+\rho\cdot N+\phi I_{12})+\alpha R_1-\mu S_1$$

$$\dot{S}_2=-\frac{\beta(t)}{N}S_2(I_1+\rho\cdot N+\phi I_{21})+\alpha R_2-\mu S_2$$

$$\dot{I}_{12}=\frac{\beta(t)}{N}S_1(I_2+\rho\cdot N+\phi I_{12})-(\gamma+\mu)I_{12}$$

$$\dot{I}_{21}=\frac{\beta(t)}{N}S_2(I_1+\rho\cdot N+\phi I_{21})-(\gamma+\mu)I_{21}$$

$$\dot{R}=\gamma(I_{12}+I_{21})-\mu R \tag{1}$$

The parameter β takes the seasonal forcing into account as a cosine function and is given explicitly by

$$\beta(t)=\beta_0\cdot(1+\eta\cdot\cos((\omega\cdot(t+\varphi)))) \tag{2}$$

where β_0 is the infection rate, η is the degree of seasonality and φ the phase which becomes important only when considering empirical time series. In this model, a susceptible individual can become infected also by meeting an infected individual from an external population (hence $(\beta/N\cdot S\cdot I)$ goes to $(\beta/N\cdot S\cdot(I+\rho\cdot N))$) contributing to the force of infection with an import parameter ρ. The parameter ϕ in our model is the ratio of secondary infection contribution to the force of infection. For instance, we study the region of the parameter $\phi<1$, which acts as decreasing the infectivity of secondary dengue infection, where the hospitalization is more likely due to the ADE effect associated with the severity of the disease. The secondary infected individuals do not contribute to the force of infection as much as people with first infection do.

The deterministic model formulation is based on the large number assumption. As a consequence the number of individuals can be used to scale all state variables of the model. The constant population $N=100$ is used for clarity so that all epidemiological proportions (susceptibles, infected and recovered) are given in percentage. The demography rate is denoted by μ and the parameter values are given in Table 1.

3. Analysis techniques

The previous analysis of the non-seasonal multi-strain dengue model has shown a rich variety of dynamics through bifurcations up to deterministically chaotic attractors in an unexpected parameter region of $\phi<1$ just by adding temporary cross-immunity to a previously existing dengue model. In Aguiar et al. (2008) a time series analysis (simulations and calculation of Lyapunov exponents) and a numerical bifurcation analysis were performed. The equilibrium values of the state variables are calculated by solving the set of non-linear equations formed by the right-hand side of the system (1) equal to zero. Often multiple equilibria coexist. The stability of each equilibrium is found by linearization, that is calculating the eigenvalues of the Jacobian matrix evaluated at that point. When all eigenvalues have negative real parts the equilibrium is stable, otherwise it is unstable. A bifurcation point is defined as a parameter value where the long-term dynamics of the system changes qualitatively at points where one eigenvalue is zero (or its real part). One important bifurcation is the Hopf bifurcation point where at a pair of conjugated eigenvalues the real parts are zero. At that point the equilibrium loses stability and the system starts to oscillate, that is where a periodic solution or limit cycle originates when a parameter is varied crossing that point. A limit cycle can be found numerically by solving a boundary value problem, whereby the boundary conditions are cyclic. Observe that the period of this solution is an additional parameter calculated along with the solution. The stability of limit cycles is determined by so-called Floquet multipliers. A limit cycle is stable when all multiplier are inside the

Table 1
Parameter set for the present multi-strain model. The temporary cross-immunity period is fixed as 6 months ($\alpha=2\ y^{-1}$) and the mean recovery period is fixed as 1 week ($\gamma=52\ y^{-1}$), as observed in dengue fever epidemiology, likewise for the other epidemiological parameters. The parameters values μ, γ, $\beta=\beta_0$, α, and ϕ that are shown in the table were used also in the analysis of the models studied in Aguiar and Stollenwerk (2007) and Aguiar et al. (2008, 2009).

Par.	Description	Values	Ref.
N	Population size	100	–
μ	Birth and death rate	1/65 y	World Population Prospects
γ	Recovery rate	$52\ y^{-1}$	World Health Organization (2009) and Gubler et al. (1981)
β_0	Infection rate	$2\cdot\gamma$	Ferguson et al. (1999)
η	Degree of seasonality	0.1–0.35	Nagao and Koelle (2008)
φ	Phase	0	–
ρ	Import parameter	$0–10^{-10}$	Nagao and Koelle (2008)
α	Temporary cross-immunity rate	$2\ y^{-1}$	Matheus et al. (2005) and Lemos, Pers comm.; Diniz, Pers comm.; Halstead, Pers comm.
ϕ	Ratio of secondary infections contributing to force of infection	Variable (<1)	Halstead (2004) and Dejnirattisai et al. (2010)

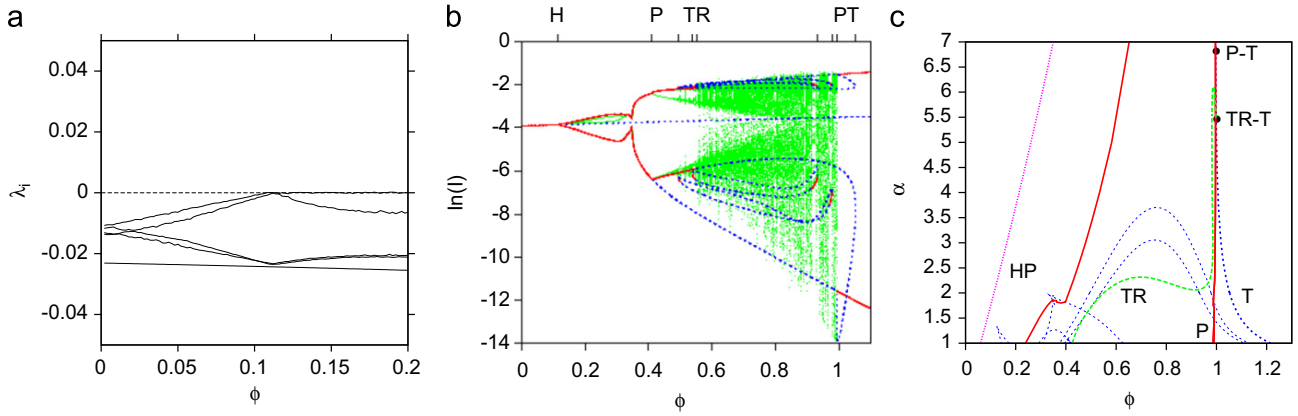

Fig. 2. Bifurcation diagram of the non-seasonal model. In (a) we show the Lyapunov spectrum ($\phi \in [0,0.2]$) with temporary cross-immunity rate $\alpha = 2$ and varying the ratio of secondary infection contribution to the force of infection ϕ. In (b) we show the one-parameter bifurcation diagram with temporary cross-immunity rate $\alpha = 2$ and varying the ratio of secondary infection contribution to the force of infection ϕ calculated using AUTO. In (c) we show the two-dimensional parameter bifurcation diagram with temporary cross-immunity rate α and the ratio of secondary infection contribution to the force of infection ϕ varying simultaneously in the range $\phi \in [0,1.3]$ and $\alpha \in [1,7]$, calculated using AUTO. In addition to the Hopf bifurcation (dotted lines) and many tangent bifurcation curves (dashed lines) the torus *TR* and pitchfork *P* bifurcations are shown. At the codim-two points $P-T$ the pitchfork and tangent bifurcations for limit cycles meet and at point $TR-T$ the pitchfork and torus bifurcations.

unit circle of the complex plane and unstable when at least one is outside. At a bifurcation point the bifurcation parameter value is such that one multiplier lies on the unit circle of the complex plane. When this multiplier equals 1 it is a tangent bifurcation while when -1 then a period-doubling (or flip) bifurcation occurs. Changing a parameter can give a cascade of period-doubling bifurcation leading to chaotic dynamics. Another important bifurcation point is the torus or Neimark–Sacker bifurcation of the limit cycle where two complex conjugate multipliers are on the unit circle. At such a point limit cycles or quasi-periodic dynamics on the torus, or chaotic dynamics originate when the bifurcation parameter is varied. For an introduction into bifurcation analysis we refer the reader to Guckenheimer and Holmes (1985), Kuznetsov (2004), and for applications in eco-epidemiological models (Malchow et al., 2008; Stiefs et al., 2009; Kooi et al., 2011).

The Lyapunov exponent is a generalization of both an eigenvalue and a Floquet multiplier. While for a fixed point the contraction and expansion rates are given by the eigenvalues and for a limit cycle by Floquet multipliers, for more complex geometrical objects (torus, chaotic attractors) the contraction and expansion rates are given by the Lyapunov exponents (Ott, 1993). For instance, the dynamics on or beyond a torus is classified as periodic, when one Lyapunov exponent zero, aperiodic when two Lyapunov exponents zero, and chaotic when one Lyapunov exponent zero and at least one positive. Lyapunov exponents can be calculated along the trajectory as

$$\lambda_i(n) = \frac{1}{n \cdot \Delta t} \ln\left(\prod_{v=1}^{n} |r_{ii}(v)| \right) \tag{3}$$

where Δt is the time-step, n the (large) number of time steps and r_{ii} are the diagonal elements of the upper triangular matrix R of the v-th QR-decomposition at the v-th time-step.

Just as with the eigenvalues of the Jacobian matrix, the number of Lyapunov exponents equals the dimension of the system (nine for system (1) and 11 for the augmented system described in Appendix A). The so-called dominant Lyapunov exponent (DLE) is the exponent with the largest magnitude. The set of Lyapunov exponents is called the Lyapunov spectrum which can be calculated for all parameter values. The situation, when all Lyapunov exponents are negative gives a stable equilibrium, one dominant zero Lyapunov exponent indicates a stable limit cycle, two dominant zero Lyapunov exponents quasi-periodicity (for instance on a torus), a positive Lyapunov exponent chaotic behavior and multiple positive Lyapunov exponent hyperchaos.

The model (1) shows a so-called $\mathbb{Z}_2$ symmetry and this leads to specific bifurcations such as the pitchfork bifurcation. We extend the analysis of the non-seasonal model with a two-parameter bifurcation analysis where both, the ratio of secondary infection contribution to the force of infection ϕ and temporary cross-immunity rate α vary simultaneously (see Fig. 2c). We used the software AUTO (Doedel and Oldeman, 2009) to calculate the bifurcation curves presented. The Lyapunov exponents were calculated using an iterated technique using the QR decomposition algorithm via Householder matrices (see Aguiar et al., 2008; Eckmann et al., 1986; Holzfuss and Lauterborn, 1989; Holzfuss and Parlitz, 1991).

Both the bifurcation analysis (for equilibria and limit cycles) and the Lyapunov spectrum calculation (for chaotic dynamics) can be done for autonomous and non-autonomous (e.g. seasonally forced) systems. With sinusoidal forcing, the non-autonomous system (1) can be coupled with the Hopf oscillator (a set of two ODE'S), to get an equivalent autonomous system of dimension 11. Notice that the period of the forcing is fixed: equal to 1, and that a steady-state solution does not exist. The basal dynamics is now a periodic solution with period equal to the forcing period, which is a limit cycle of the equivalent autonomous system. Hence the dynamics can be analyzed in the same way as described above and shown in the Appendix A.

4. Bifurcation analysis

In this section we start with a bifurcation analysis of the non-seasonal model and then continue with two scenarios of seasonally forced systems, namely the low seasonal model and the high seasonal model with a low import of infected individuals.

4.1. Bifurcation analysis of the non-seasonal model

In this section we show briefly the results for the non-seasonal system published in Aguiar et al. (2008, 2009) on which the further results of the present article are based. First we show in Fig. 2(a) the Lyapunov exponents in the parameter range $\phi \in [0,0.2]$. The DLE is negative below and becomes zero at

$\phi = 0.108$, the Hopf bifurcation point which is also predicted by AUTO (Doedel and Oldeman, 2009).

Second, we show the one-parameter bifurcation diagram for $\phi \in [0,1.3]$ (see Fig. 2(b)). At fine grid in this parameter range, system (1) was solved numerically. We discarded 2000 years of transients and plot the varying ratio of the secondary infection contribution to the force of infection (ϕ) over the steady state or local maxima of logarithm of total number of infected ($\ln(I)$, where $I := I_1 + I_2 + I_{12} + I_{21}$), obtaining the one-parameter bifurcation diagram.

The one-parameter diagram is shown in Fig. 2(b). Here the logarithm of total number of infected are shown, where solid lines denote stable equilibria or limit cycles, and dashed lines unstable equilibria or limit cycles. Various bifurcations are: Hopf bifurcation $H(\phi = 0.11326)$, pitchfork bifurcations $P(\phi = 0.41145$, 0.99214), torus bifurcation $TR(\phi = 0.55069)$ and tangent bifurcations $T(\phi = 0.4.9406, 0.53874, 0.93103, 0.97825, 1.05242)$.

In addition to this main bifurcation pattern we found two isolas, consisting of isolated limit cycles existing between two tangent bifurcations (for more information on the isolas see Aguiar et al., 2009). At the Hopf bifurcation H ($\phi = 0.1133$) the stable fixed equilibrium becomes an unstable fixed equilibrium and in the parameter interval between the Hopf bifurcation and the pitchfork bifurcation P ($\phi = 0.4114$) there is a symmetric stable limit cycle (for more information on the bifurcation analysis by continuation for the non-seasonal multi-strain model see Aguiar et al. (2008, 2009), however, in these articles it is wrongly stated that it is a fixed limit cycle instead of the symmetric limit cycle). At a pitchfork bifurcation point, the symmetric limit cycle becomes unstable and remains symmetric, while two stable S-conjugate limit cycles originate (see Kuznetsov, 2004, Theorem 7.7). These S-conjugate limit cycles become unstable at a torus bifurcation TR ($\phi = 0.5507$). At this torus or Neimark–Sacker bifurcation the dynamics becomes chaotic (positive Lyapunov exponent). Increasing the ratio of secondary infection contribution to the force of infection (ϕ) further, this chaotic behavior disappears at a second pitchfork bifurcation P ($\phi = 0.9921$). At this pitchfork bifurcation the branch of limit cycles that was originated at the first pitchfork bifurcation terminates after going through a region where two limit cycles coexist and disappear at a tangent bifurcation. In the small ϕ interval between the pitchfork bifurcation and the tangent bifurcation T ($\phi = 0.931$) two stable limit cycles coexist. This means that the stable manifold of the unstable intermediate limit cycle forms the separatrix for the two basins of attraction in the state space. We remark that the sudden disappearance of the chaotic attractor at the pitchfork bifurcation is similar to the classical intermittency route to chaos occurring at for instance a tangent bifurcation.

Fig. 2(c) gives the most important bifurcation curves where both ϕ and α vary simultaneously: for an equilibrium the Hopf bifurcation H, and for limit cycles the torus-bifurcation TR and the pitchfork bifurcation P and a tangent bifurcation T. At the two codim-two points, $P-T$ and $TR-T$, the tangent bifurcation for a limit cycle splits off a pitchfork and a torus bifurcation. This diagram shows for which ϕ and α parameter values chaotic behavior can occur, namely below the torus-bifurcation TR and on the left hand side of the pitchfork bifurcation P that originates from the $P-T$ point. However, within this region there are periodic windows such as shown in Fig. 2(b). We found isolas coexisting with the attractors of this main bifurcation structure. A stable limit cycle was calculated by simulation starting from initial values in the state space obviously outside the basin of attraction of the attractors of the main bifurcation structure. Continuation starting from this limit cycle gave rise to bifurcations into chaos. For a detailed analysis of the attractors in state space for the non-seasonal model, see also Appendix B.1 and Aguiar et al. (2008, 2009).

By adding a low import factor into the non-seasonal model the classical ADE chaotic region for $\phi > 1$ found in Ferguson et al. (1999) and Aguiar et al. (2008) disappears (see Appendix C, Fig. C1).

4.2. Bifurcation analysis of the seasonal models

In this section we relate and compare the results for the seasonally forced systems to that of the non-seasonal system discussed in the previous section. First we compare the bifurcation diagrams obtained for the non-seasonal and seasonal models. In the special case where $\eta = 0$ the seasonal system is decoupled in the original non-seasonal system studied in Aguiar et al. (2008, 2009) with $\beta = \beta_0$ and the augmented oscillator described in Appendix A, by system (A.1). It is easy to show that the augmented system with (A.1) is $\mathbb{Z}_2$-symmetric just as the original seasonal system (1). This has consequences for the type of bifurcations to be expected. If the non-seasonal system possesses a Hopf bifurcation, the seasonally forced system has a torus bifurcation.

The bifurcation diagrams for the seasonal models are shown in Fig. 3(a) and (b). In Fig. 3(a) the bifurcation diagram for the system with low seasonality ($\eta = 0.1$) is not very informative since we have many local extrema even for the most simple case of the torus. When increasing the ratio of secondary infection contribution to the force of infection (ϕ values), the troughs become very low, with the logarithm of total infected going as low as -160. By adding a low import of infected ($\rho = 10^{-10}$) into the seasonal model, the logarithm of total infected does not pass below -16 (see Fig. 3(b)), avoiding the chance of extinction in stochastic systems with reasonable system size.

In order to get more insight about the disappearance of the chaotic behavior we study a two-parameter diagram (see Fig. 4) for each one of the models (non-seasonal, low seasonal and high seasonal with import of infected), where the ratio of the secondary infection contribution to the force of infection ϕ and the temporary cross-immunity rate α are varied simultaneously. The time series simulations (Section 5) and state space plots (Appendix B) are also analyzed and the results are compared for the different case scenarios.

4.2.1. Bifurcation analysis of the low seasonal model

For the non-seasonal system, with 6 months of temporary cross-immunity ($\alpha = 2\ \mathrm{y}^{-1}$), there is a stable equilibrium that becomes unstable at a super-critical Hopf bifurcation H at ($\phi = 0.1133$) leading to a stable limit cycle for higher ϕ values. By adding low seasonal forcing ($\eta = 0.1$) into the system, a torus bifurcation TR appears at $\phi = 0.1145$, slightly above the Hopf bifurcation of the non-seasonal system. When a low import factor ($\rho = 10^{-10}$) of infected is included into the high seasonal system ($\eta = 0.35$), the torus bifurcation TR is predicted by AUTO at $\phi = 0.13$.

These results show that on the right-hand side of the torus bifurcation TR possibly chaotic dynamics can occur. Therefore we continue our analysis with the calculation of the Lyapunov exponent spectrum in Fig. 5.

Fig. 5(a) shows the Lyapunov spectrum in the parameter range $\phi \in [0,1.2]$ for the low seasonal model where $\eta = 0.1$. The DLE in the chaotic area goes up to $\lambda = 2$ where the prediction horizon of the monthly peaks in the time series is in the range of half a year. In Fig. 5(b) the Lyapunov exponents are depicted in the parameter range $\phi \in [0,0.2]$. There is a stable periodic solution which becomes unstable at a torus bifurcation. Using AUTO we calculated a torus bifurcation TR at $\phi = 0.1145$, slightly above the Hopf

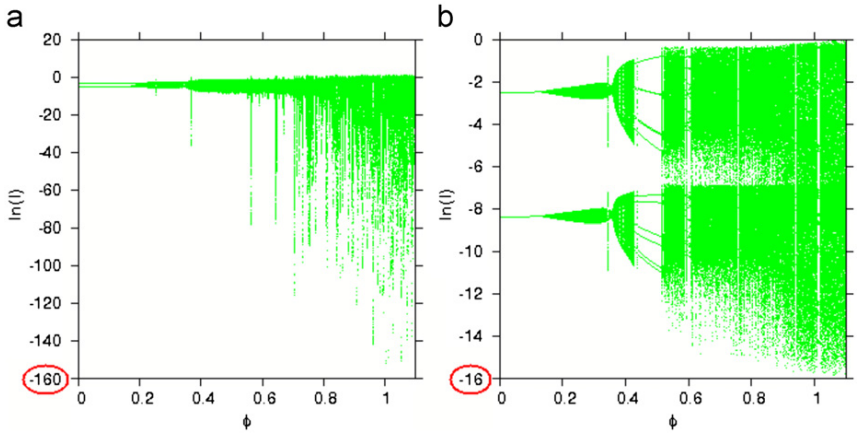

Fig. 3. Bifurcation diagram comparison between seasonal models. In (a) bifurcation diagram for the low seasonal model without import of infected, where the degree of seasonality $\eta = 0.1$ and in (b) bifurcation diagram for the high seasonal model with a low import of infected. Here, the degree of seasonality $\eta = 0.35$ and the import factor $\rho = 10^{-10}$. These bifurcation diagrams can be compared with Fig. 2(b) for the non-seasonal model ($\eta = 0$). The other parameter values are listed in Table 1. Notice that in the case (a) with low seasonality and no import the infected go to very low numbers, unrealistically low for any empirical epidemiological system.

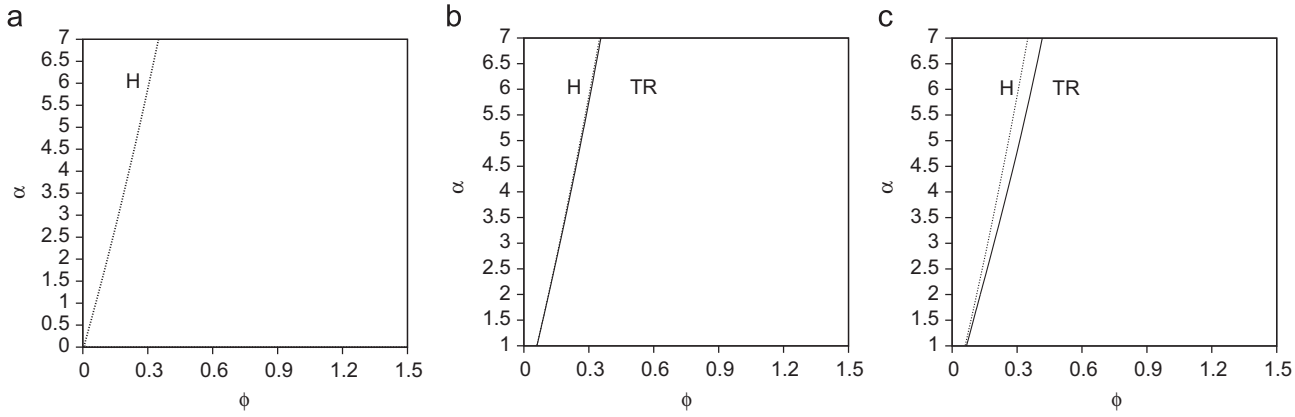

Fig. 4. Two-dimensional parameter bifurcation diagram with the ratio of secondary infection contribution to the force of infection ϕ and temporary cross-immunity rate α as bifurcation parameters. In (a) the Hopf bifurcation line for the non-seasonal model, i.e. $\eta = 0$, in (b) the torus bifurcation line for the low seasonal model, i.e. $\eta = 0.1$ is close to the Hopf bifurcation line for the non-seasonal model ($\eta = 0$) and in (c) the torus bifurcation line for the high seasonal model with low import, i.e. $\eta = 0.35$, $\rho = 10^{-10}$, in comparison with the Hopf bifurcation line for the non-seasonal model ($\eta = 0$).

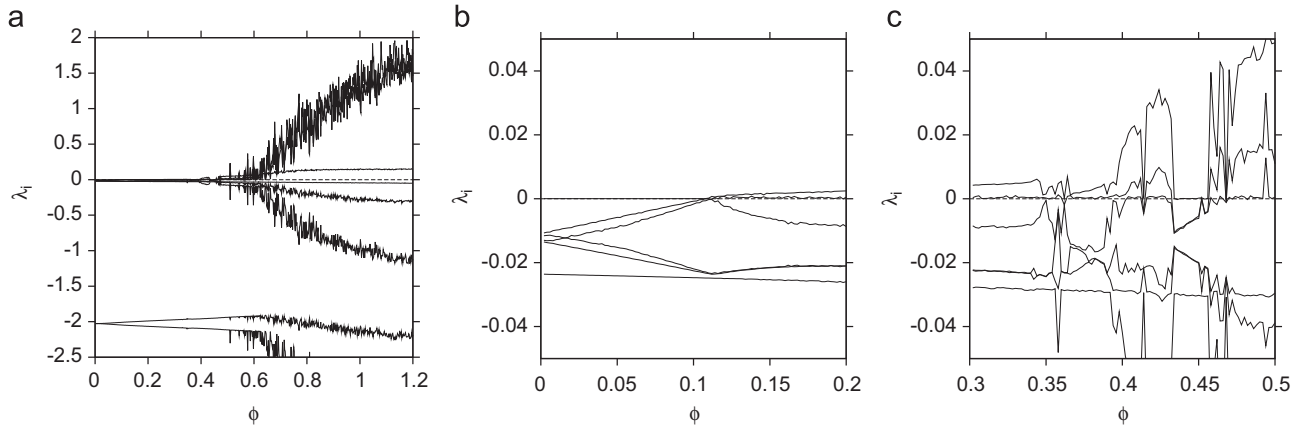

Fig. 5. For the low seasonal system, where temporary cross-immunity rate $\alpha = 2$, the recovery rate $\gamma = 52\ y^{-1}$, the infection rate $\beta_0 = 2 \cdot \gamma$, the degree of seasonality $\eta = 0.1$ and birth and death rate $\mu = 1/65$ y, in (a) the Lyapunov spectrum for the ratio of secondary infection contribution to the force of infection $\phi \in [0,1.2]$, the whole parameter region of interest, in (b) Lyapunov exponents for small values of the ratio of secondary infection contribution to the force of infection $\phi \in [0,0.2]$, and in (c) Lyapunov exponents for the ratio of secondary infection contribution to the force of infection $\phi \in [0.3,0.5]$, the parameter region of onset of complexity.

bifurcation of the non-seasonal system at ($\phi = 0.1133$). Observe that the torus bifurcation *TR* in the seasonally forced system is close to the Hopf bifurcation for the non-seasonal system. This is reasonable since seasonal forcing adds complexity to the dynamics behavior, i.e. an equilibrium becomes a periodic solution and a limit cycle becomes a solution on a torus, whether

periodic (one Lyapunov exponent zero), aperiodic (two Lyapunov exponents zero) or chaotic (one Lyapunov exponent zero and at least one positive). For higher ϕ values the solution is restricted to the torus or a chaotic attractor.

In Fig. 5(c) the Lyapunov exponents are depicted in the parameter range $\phi \in [0.3,0.5]$ for the same low seasonal case of $\eta = 0.1$. There is a window in the chaotic region for ϕ-values above the torus bifurcation *TR* around $\phi = 0.44$ where there is a single Lyapunov exponent equal to zero, suggesting the existence of a stable limit cycle, which implies phase-locking. Continuation of this solution with ϕ as free parameter reveals that this cycle that is a period-13 cycle possesses a tangent bifurcation at $\phi = 0.431$ and a torus bifurcation at $\phi = 0.471$. These two critical points enclose the period-13 window of stable periodic solutions.

For detailed analysis on the attractors in state space for the low seasonal, see Appendix B.2.

4.2.2. Bifurcation analysis of the high seasonal model with import

In the analysis of the high seasonal model ($\eta = 0.35$) with low import of infected individuals ($\rho = 10^{-10}$), AUTO predicted a torus bifurcation *TR* at $\phi = 0.13$. In Fig. 6(a) a little below that point the DLEs become positive, indicating chaos. The discrepancies between the continuation versus Lyapunov exponents calculation techniques happen due to long transients and consequently long sampling times in the Lyapunov exponents calculation near bifurcation points where one exponent becomes close to zero.

Another interesting range of ϕ is a window in the chaotic region around $\phi = 0.44$ where a stable limit cycle with period 12 exists. Hence in this region phase-locking occurs. With AUTO we calculated a tangent bifurcation at $\phi = 0.406$ and a torus bifurcation at $\phi = 0.522$. The torus bifurcation is also predicted very well comparing the results given in Fig. 6(b), where the second zero Lyapunov exponent appears at $\phi = 0.522$. The position of the tangent bifurcation at $\phi = 0.406$ is less clear from this figure obviously due to numerical inaccuracies prone to the detection of bifurcation points via integration in time instead of the calculation of the limit cycle by using a boundary value problem and the calculation of the Floquet multipliers.

In the limiting case where the amplitude of the seasonal forcing is zero, the torus bifurcation *TR* of the seasonally forced system coincides with the Hopf bifurcation *H* of the non-seasonal system. The larger the amplitude of the seasonal forcing η, the higher the effects where the torus bifurcation occurs at higher ϕ values. The same effect is found when adding the import factor of infected ρ into the seasonal system.

For detailed analysis on the attractors in state space for the high seasonal model with import, see Appendix B.3.

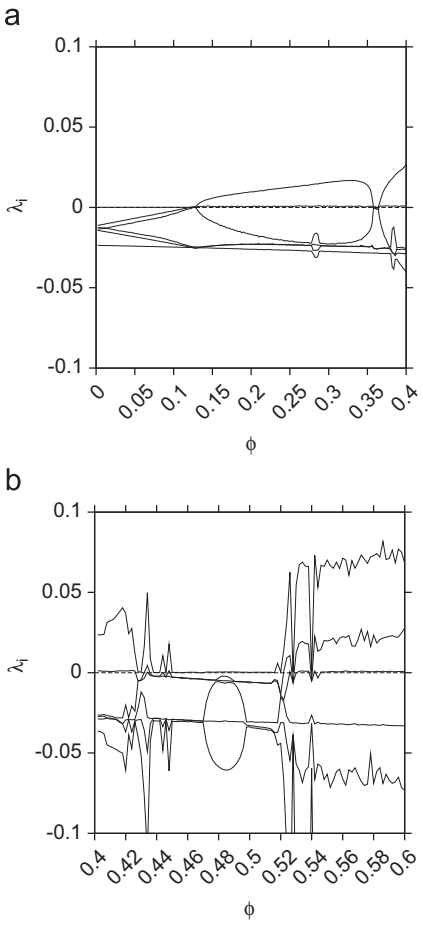

Fig. 6. For the high seasonal system ($\eta = 0.35$) with a low import of infected ($\rho = 10^{-10}$), in (a) Lyapunov exponents for the ratio of secondary infection contribution to the force of infection $\phi \in [0,0.4]$. The second zero Lyapunov exponent is at $\phi = 0.128$, just before the torus bifurcation point calculated by AUTO at $\phi = 0.13$. In (b) Lyapunov exponents for the ratio of secondary infection contribution to the force of infection $\phi \in [0.4,0.6]$. In this region a tangent bifurcation at $\phi = 0.406$ and a torus bifurcation at $\phi = 0.522$ is predicted by AUTO.

5. Time series

This study is completed with a time series analysis where the results are shown, leading to a discussion on its implications for data analysis. For the seasonal forcing to be inserted into system (1) we use Eq. (2) with $\omega = 2\pi \cdot 1/T$ and $T = 1$ y as monitoring data of dengue suggest. For the moment we assume perfect sinusoidal forcing without any phase shift, hence $\varphi = 0$.

In this section, we compare the time series simulations and respective state space plots for the number of susceptible versus logarithm of the overall infected for the non-seasonal and seasonal scenarios. For a population $N = 100$, where the initial conditions are given by $S = 70$, $I_1 = 20$, $I_2 = 10$, and $R_1, R_2, S_1, S_2, I_{12}, I_{21}, R = 0$, fulfilling the condition of constant population size $N = S + I_1 + I_2 + R_1 + R_2 + S_1 + S_2 + I_{12} + I_{21} + R$, we discarded 5000 years of transients. The following parameters are fixed as shown in Table 1, temporary cross-immunity rate $\alpha = 2\ \mathrm{y}^{-1}$, recovery rate $\gamma = 52\ \mathrm{y}^{-1}$, infection rate $\beta_0 = 2 \cdot \gamma$, seasonality $\eta = 0.35$, import factor $\rho = 10^{-10}$, birth and death rate $\mu = 1/65$ y and the ratio of secondary infection contribution to the force of infection $\phi = 0.9$, as initial attempt for the parameter estimation (Aguiar et al., accepted).

In Fig. 7(a) the time series simulation results for the total number of infected ($I_1 + I_2 + I_{12} + I_{21}$) in the non-seasonal system, previously studied in Aguiar et al. (2008), is shown. Besides showing an irregular pattern of outbreaks that happens every 5 years, the non-seasonal system and its time series are not able to represent dengue fever epidemiology that is characterized as a yearly cycle of incidences. By adding low seasonality into the system, the epidemic outbreaks appear every year (see Fig. 7(b)). However, between two large outbreaks there is a very low number of cases in subsequent years, which is also not data alike (see Fig. 9(a), for example).

In Fig. 7(c), the time series simulation in the high seasonal system with a low import of infected contributing to the force of infection is shown. The addition of import into the seasonal system gives a much more realistic pattern of dengue fever epidemics, with irregular, yearly and smooth outbreaks. The system has a reasonable size (the number of infected stays quite away from zero), avoiding the chance of extinction in stochastic systems. Observe that very high import of infected only leads to

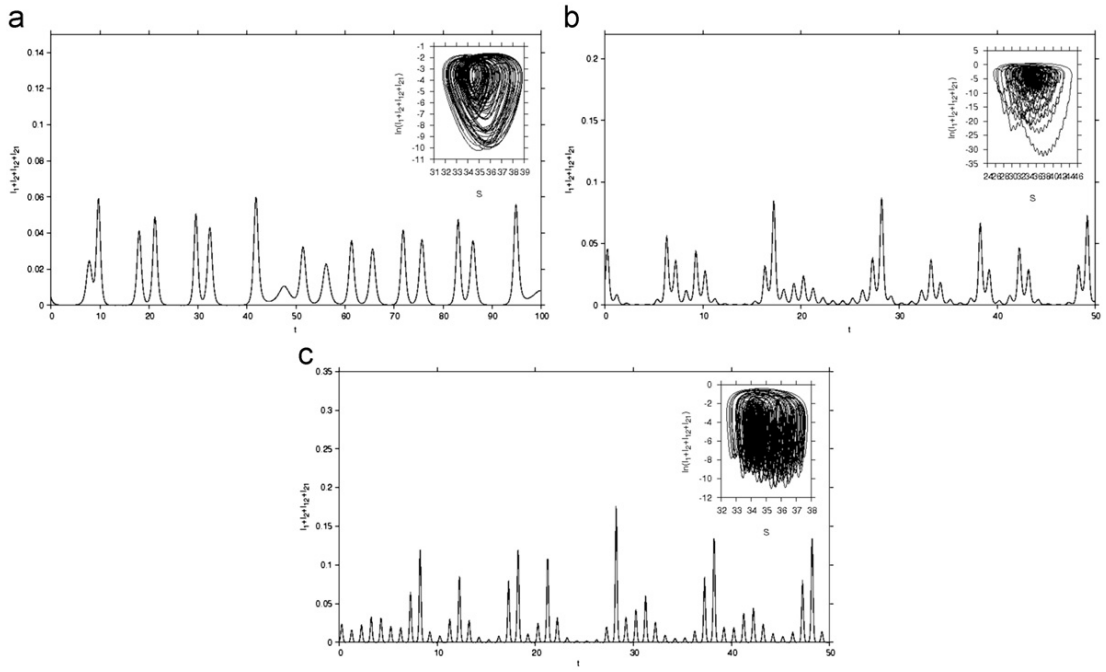

Fig. 7. Time series simulations. In (a) time series simulation for the non-seasonal model ($\eta = 0$). In (b) time series simulation for the low seasonal model, with seasonality $\eta = 0.1$ and the phase $\varphi = 0$. In (c) time series simulation for the seasonal model with a low import of infected. Here, the degree of seasonality $\eta = 0.35$, the phase $\varphi = 0$, and the import of infected $\rho = 10^{-10}$. The absolute numbers on the y-axes indicate percentage of the total population.

periodic solution, whereas for import of $\ln(\rho) \approx -18$ and below, complex behavior is observed (see Appendix D, Fig. D1).

5.1. Lyapunov exponents and predictability

In this section, the Lyapunov spectrum for both the non-seasonal model and the seasonal model with import are shown and compared concerning the prediction horizon of the monthly peaks in the multi-strain dengue model time series. We take as an example the DLE for $\phi = 0.9$ in the region where the system is chaotic (positive DLE). Fig. 8(a) shows the Lyapunov spectrum for the non-seasonal system previously studied in Aguiar et al. (2009). There are only negative exponents where the ratio of secondary infection contribution to the force of infection ϕ is in the interval (0,0.106) indicating a steady state point dynamic. At $\phi = 0.108$ the DLE is zero (up to certain numerical accuracy of order 10^{-5}), indicating a periodic solution (period one or limit cycle dynamic). At $\phi = 0.516$ the DLE becomes consistently positive, indicating chaotic behavior up to $\phi = 0.994$. The low noisy level of the second largest Lyapunov exponent around its theoretical value of zero, indicates that the DLE is really positive. For ϕ in the interval (0.994, 1.2) the system gets stabilized again showing only periodic solutions (zero DLE). For the chaotic region of $\phi = 0.9$, the DLE$=0.04$ giving ≈ 25 y of prediction horizon in the monthly time series (see Fig. 8(b)). In order to get a qualitative insight into the predictability in the monthly sampled time series, i.e. to show how the original system behaves under a small perturbation we plot two different trajectories of the same system (for the non-seasonal model in Fig. 8b), and for the high seasonal model with a low import of infected in Fig. 8(d), where the perturbed system (black line) is compared with the original model simulation (red line). To get the trajectory of the perturbed system, we keep the last point of the transient of the original system and use those values as starting values to compute the new and perturbed trajectory. The perturbation is given by $S = S + R \cdot \varepsilon$ and $R = R \cdot (1.0 - \varepsilon)$, where $\varepsilon = 0.001$.

The same exercise was done for the seasonal model with low import of infected (see Fig. 8(c) and (d)). For the seasonal system with import, the zero Lyapunov exponent is visible indicating a period one dynamic from ϕ between 0 and 0.122 where another slightly positive exponent appears ($\lambda = 0.000145$). From ϕ between 0.122 and 1.2 we have complex dynamics with torus bifurcations (two zero exponents) up to hyperchaos (two positive exponents). The chaotic region of $\phi = 0.9$, shows the DLE$=0.118$ giving ≈ 8.5 y of prediction horizon in the monthly time series. It is clear that the addition of seasonal forcing into the system by itself decreases the practical predictability (see Fig. 5(a)), however, the addition of a low import into the seasonally forced system helps to get a more complex dynamics and a better prediction horizon in the monthly time series.

5.2. Implications for data analysis

Physicians in Thailand are trained to recognize and treat dengue fever and practically all cases of DHF and DSS are hospitalized. A system for reporting communicable diseases including DHF/DSS was considered fully installed in 1974 and the data bank of DHF and DSS is available at the Ministry of Public Health, Bangkok (Chareonsook et al., 1999). Thailand is the world's 50th largest country in terms of total area, and the 20th most-populous country, with approximately 66 million people. Thailand is divided into 75 provinces (changwat) plus the capital Bangkok which is a special administrative area. The provinces are geographically grouped into six regions, North, North-East, West, Central, East, and South Wikipedia contributors. The inspection of the available DHF incidence data in Thailand shows a smooth behavior with a well defined maximum each year of irregular hight, for the North, North-East, and West Provinces (see Fig. 9a) for example, the DHF incidence data for Chiang Mai Province) whereas for the Central, East, and South Provinces the data is very noisy linked with a low endemicity of DHF cases. We take the Province of Chiang Mai as a case study where the empirical DHF

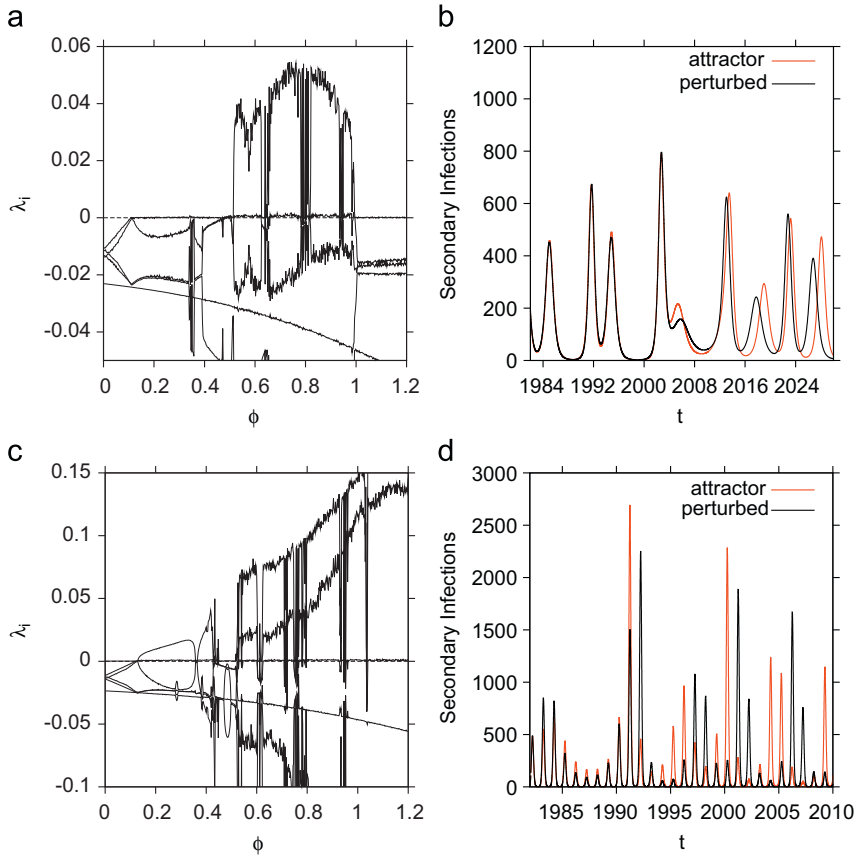

Fig. 8. Qualitative insight into the predictability in the monthly time series. In (a) we show the Lyapunov spectrum for the non-seasonally forced dengue model where the first five Lyapunov exponents are given. The DLE in the chaotic region of the ratio of secondary infection contribution to the force of infection $\phi = 0.9$ is $\lambda = 0.04$ giving ≈ 25 y of prediction horizon in the monthly time series. In (b) the monthly time series simulation for $\phi = 0.9$ is shown where the original trajectory (red line) is compared with the perturbed trajectory (black line). In (c) we show the Lyapunov spectrum for the high seasonal model ($\eta = 0.35$) with import ($\rho = 10^{-10}$) where the first five Lyapunov exponents are given. Here, the DLE in the chaotic region of the ratio of secondary infection contribution to the force of infection $\phi = 0.9$ is $\lambda = 0.118$ giving ≈ 8.5 y of prediction horizon in the monthly time series. In (d) we show the monthly time series simulation for $\phi = 0.9$ where the original trajectory (red line) is compared with the perturbed trajectory (black line). For the other parameter values used here see Table 1. (For interpretation of the references to color in this figure legend, the reader is referred to the web version of this article.)

incidence data and the time series simulation for the seasonal model with import (see Fig. 9(b)) are compared (see Fig. 9(c)).

The seasonal model with import shows complex dynamics and qualitatively a very good result when comparing empirical DHF and simulation results. However, the extended model needs to be parameterized on data referring to incidence of severe disease (Aguiar et al., accepted). The ability to predict the future of the dengue outbreaks by analyzing the available epidemiological data via mathematical models ultimately aims to provide a tool to guide policies of prevention and control of the dengue virus transmission, including the implementation of vaccination programs when the dengue fever vaccine will be accessible.

6. Discussion and conclusions

In this manuscript a comparative study between three different scenarios (non-seasonal, low seasonal and high seasonal with a low import of infected individuals) was performed. The role of seasonality and import of infected individuals in such systems were considered as biologically relevant effects determining the dynamical behavior of the system.

We integrated the use of numerical bifurcation analysis and time series analysis techniques for the study of the longterm dynamics of the non-autonomous system. Then the Lyapunov exponent is a generalization of both an eigenvalue and a Floquet multiplier being used for the stability analysis of respectively equilibria and limit cycles and used directly for the determination of aperiodic or chaotic attractors.

Different extensions of the classical single-strain SIR model show a rich dynamic behavior. Multi-strain dynamics has previously been demonstrated to show critical fluctuations with power law distributions of disease cases, exemplified in meningitis epidemiology (Stollenwerk and Jansen, 2003; Stollenwerk et al., 2004). Dengue models including multi-strain interactions via ADE but without temporary cross-immunity period e.g. Ferguson et al. (1999), Schwartz et al. (2005), and Billings et al. (2007) have also shown deterministic chaos when strong infectivity on secondary infection was assumed ($\phi > 1$). The addition of temporary cross-immunity period in such models, shows also a new deterministically chaotic attractor in an unexpected parameter region of reduced infectivity on secondary infection ($\phi < 1$) (Aguiar and Stollenwerk, 2007; Aguiar et al., 2008, 2009), i.e. deterministic chaos was found in a wider parameter regions. When a low import of infected individuals is introduced into this system, the chaotic dynamics for $\phi > 1$ disappears, whereas for the parameter region of $\phi < 1$ the chaotic dynamics remains (see Appendix C, Fig. C1).

In Stone et al. (2007) the seasonally forced SIR system can show already deterministic chaos. Similarly the introduction of seasonally forcing widens the parameter range of ϕ where chaotic dynamics

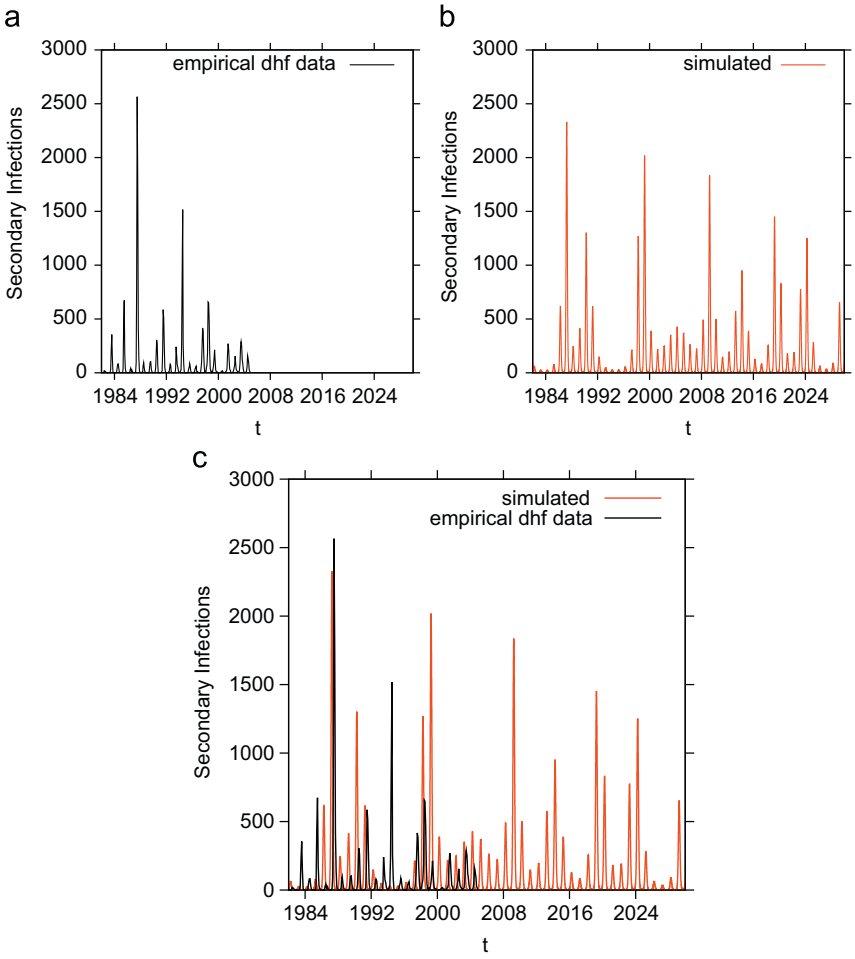

Fig. 9. In (a) we show the time series of DHF incidence in the Province of Chiang Mai in the North of Thailand. The population size is 1,649,457 (Chareonsook et al., 1999). In (b) we show a simulation for the seasonal dengue model with import. We plot the secondary infections ($I_{12}+I_{21}$) over time. The initial conditions and parameters were fixed as it follows. $N=1{,}650{,}000$, $S=1{,}250{,}000$, $I_1=250,000$. 5000 years of transients were discarded. The temporary cross-immunity rate is $\alpha=2\ \mathrm{y}^{-1}$, the recovery rate $\gamma=52\ \mathrm{y}^{-1}$, the infection rate $\beta_0=2\cdot\gamma$, the ratio of secondary infection contribution to the force of infection $\phi=0.9$, the birth and death rate $\mu=1/65$ y, seasonality $\eta=0.35$, the phase $\varphi=0$, and the import factor $\rho=10^{-10}$. In (c) empirical DHF incidence data are matched with the seasonal two-strain model with import simulation.

occurs, again also for $\phi>1$. Therefore, it is clear that the addition of seasonal forcing into the system decreases the practical predictability of the dynamical system (see Section 5.1). However, in order to be able to reproduce signals of a yearly cycle in dengue incidence, the addition of seasonal forcing is essential. However, using the same parameter set as in Aguiar et al. (2008) and including a seasonal forcing and a low import of infected individuals into our previous model (Aguiar et al., 2008) we get already a qualitatively very good result when comparing empirical DHF data and simulation results. Together with an import of $\ln(\rho)\approx -18$ and below, the system shows the expected complex dynamics (see Appendix D, Fig. D1) to explain the fluctuations observed in the available empirical data (see Fig. 9(c)).

This suggests that this parameter set can be the starting set for a more detailed parameter estimation procedure. Such a technical parameter estimation is notoriously difficult for chaotic time series but temporally local approaches are possible (Ionides et al., 2006; He et al., 2010).

Being able to predict future outbreaks of dengue in the absence of human interventions is a major goal if one wants to understand the effects of control measures. Even after a dengue virus vaccine has become accessible, this holds true for the implementation of a vaccination program. For example, to perform a vaccine trial in a year with normally low numbers of cases would make statistical tests of vaccine efficacy much more difficult than when it was performed in a year with naturally high numbers of cases. Thus predictability of the next season's height of the dengue peak on the basis of deterministic balance of infected and susceptible would be of major practical use.

Acknowledgments

We would like to thank Bernard Cazelles, Ecole Normale Supérieure, France, for providing the available DHF incidence data in Thailand. Yoshiro Nagao, Osaka University Graduate School of Medicine in Japan, and Katia Koelle, Biology Department of Duke University in the USA for providing the extended Thailand DHF incidence data, Francisco Lemos and Sonia Diniz, Belo Horizonte, Minas Gerais, and Scott Halstead, Bethesda, Maryland, for detailed information about dengue epidemiology. Maíra Aguiar also acknowledge the financial support from the FCT grants with reference SFRH/BD/43236/2008. This work has been further supported by the European Union under FP7 in the EPIWORK project and the Portuguese FCT project PTDC/MAT/115168/2009.

Appendix A. Seasonal forcing

In order to be able to use computer packages for autonomous systems such as AUTO (Doedel and Oldeman, 2009), the equation system (1) can be augmented with the following two equations:

$$\dot{x} = -\omega y + c \cdot x(\eta^2 - (x^2+y^2)) \tag{A.1}$$

$$\dot{y} = \omega x + c \cdot y(\eta^2 - (x^2+y^2)) \tag{A.2}$$

hence, a Hopf oscillator. The stable periodic solution of system (A.1) reads

$$x(t) = \eta \cdot \cos(\omega t), \quad y(t) = \eta \cdot \sin(\omega t) \tag{A.3}$$

and is without shift $\varphi = 0$ when choosing appropriate initial conditions ($x(t_0) = \eta$, $y(t_0) = 0$). This sinusoidal signal $x(t)$ is fed into the epidemic model (1) in

$$\beta(t) = \beta_0 \cdot (1 + x(t)). \tag{A.4}$$

The augmented system (1) and (A.1) is $\mathbb{Z}_2$-symmetric just as the original non-seasonal and seasonal system.

The constant $c > 0$ in the Hopf oscillator does not influence the solution $(x(t),y(t))$ in stationarity, but only the convergence toward it, hence controls the stability of the Hopf oscillation and leaves the system (1) unchanged. The Hopf oscillator can be solved explicitly in polar coordinates, hence $x = r \cdot \cos(\vartheta)$ and $y = r \cdot \sin(\vartheta)$, or inverted $r = \sqrt{x^2+y^2}$ and $\vartheta = \arctan(y/x)$.

The ODE system is in polar coordinates given by

$$\dot{r} = c \cdot r(\eta^2 - r^2) \tag{A.5}$$

$$\dot{\vartheta} = \omega \tag{A.6}$$

and solutions are

$$r(t) = \eta \left(1 - \left(1 - \frac{\eta^2}{r_0^2}\right) e^{-2\eta^2 c(t-t_0)}\right)^{-1/2} \tag{A.7}$$

$$\vartheta(t) = \vartheta_0 + \omega(t - t_0) \tag{A.8}$$

From this we can get the solution in Cartesian coordinates

$$\tilde{x}(t) = \eta \cdot \cos(\vartheta(t)), \quad \tilde{y}(t) = \eta \cdot \sin(\vartheta(t)) \tag{A.9}$$

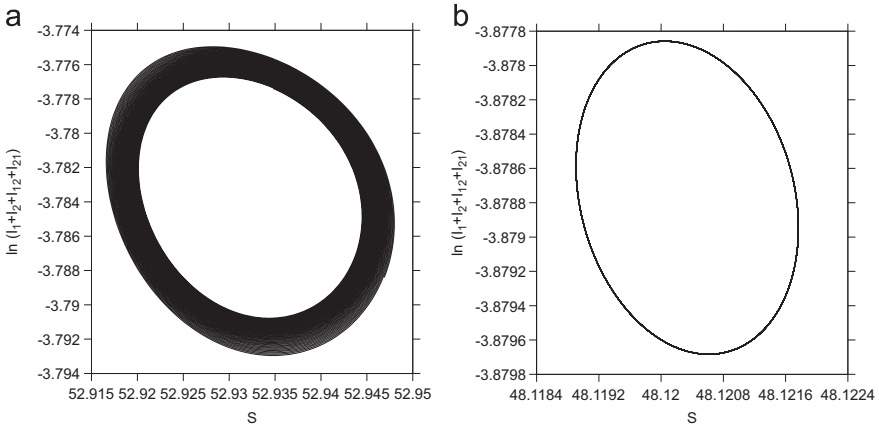

Fig. B1. Attractors in state space for the non-seasonal model. We plot the susceptibles S over the logarithm of total number of infected $I_1+I_2+I_{12}+I_{21}$. In (a) the state space plot for $\phi = 0.1133$, the Hopf bifurcation point calculated by AUTO. Two thousand years of transients were discarded, insufficient to obtain the expected simple limit cycle. In (b) the attractor for $\phi = 0.1133$. It is really a limit cycle after discarding a sufficiently long transient of 40,000 years.

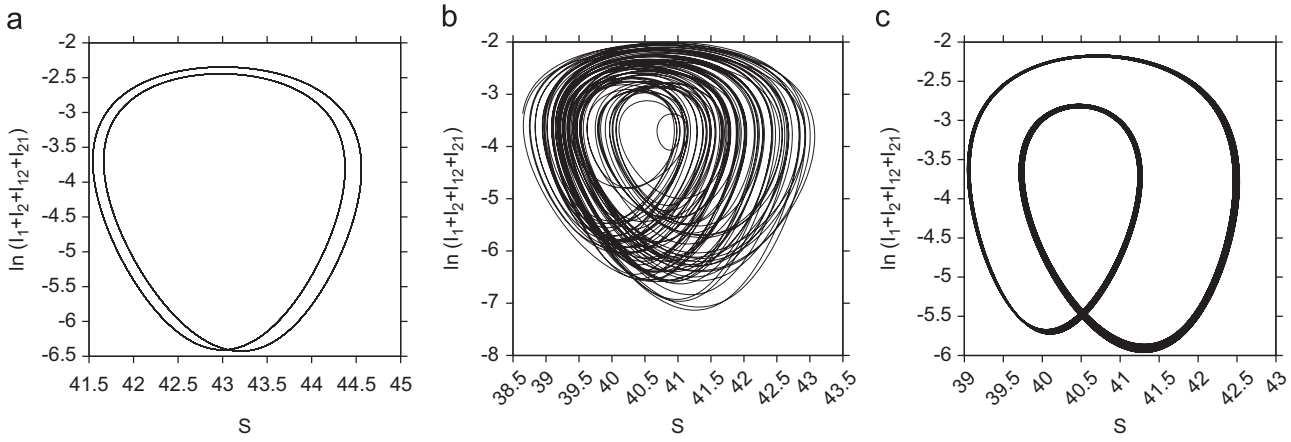

Fig. B2. Attractors in state space for the non-seasonal model. In (a) the attractor for $\phi = 0.4115$ with 2000 years of transients discarded, the pitchfork bifurcation point calculated by AUTO. In (b) a chaotic attractor, and in (c) a torus attractor both found for $\phi = 0.5507$. Those attractors were stable for very long transients of 10,000 years suggesting a coexistence of attractors.

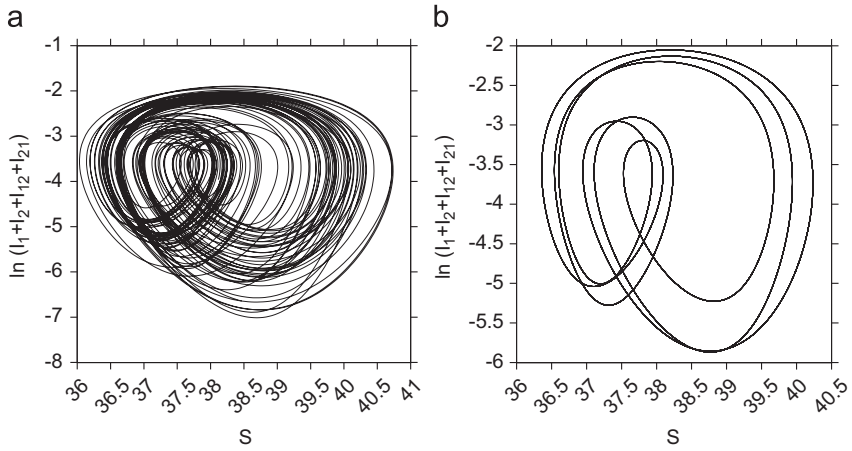

Fig. B3. Attractors in state space for the non-seasonal model. In (a) the chaotic attractor from the main bifurcation branch, and in (b) a coexisting attractor for in the isola region, both when $\phi = 0.71$. The coexistence of attractors was found when changing the initial conditions.

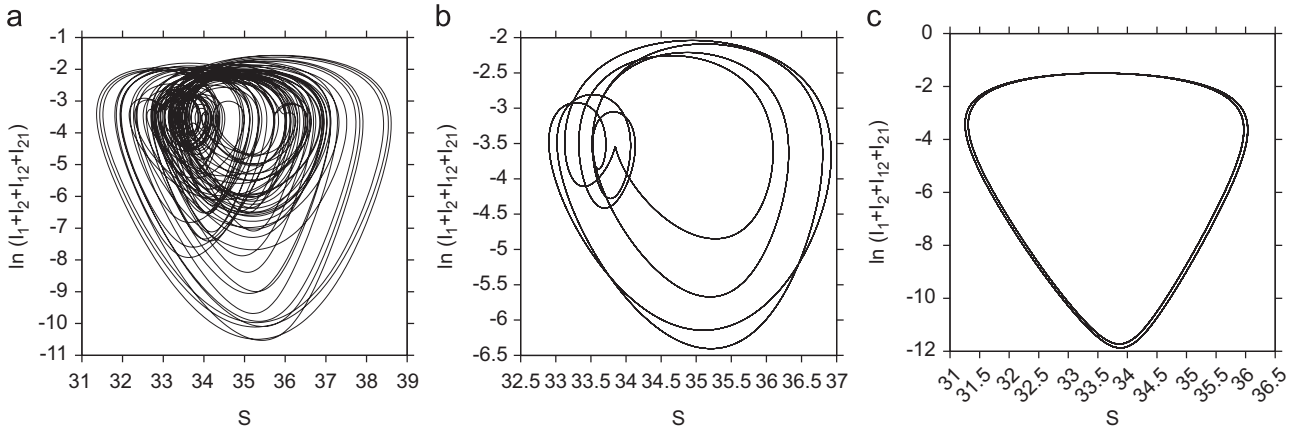

Fig. B4. Attractors in state space for the non-seasonal model. The same as before, in (a) the chaotic attractor, in (b) the coexisting attractor at $\phi = 0.934$. The coexistence of attractors was found when changing the initial conditions. In (c) attractor with two limit cycles coexisting in $\phi = 0.9921$, the pitchfork bifurcation point calculated by AUTO.

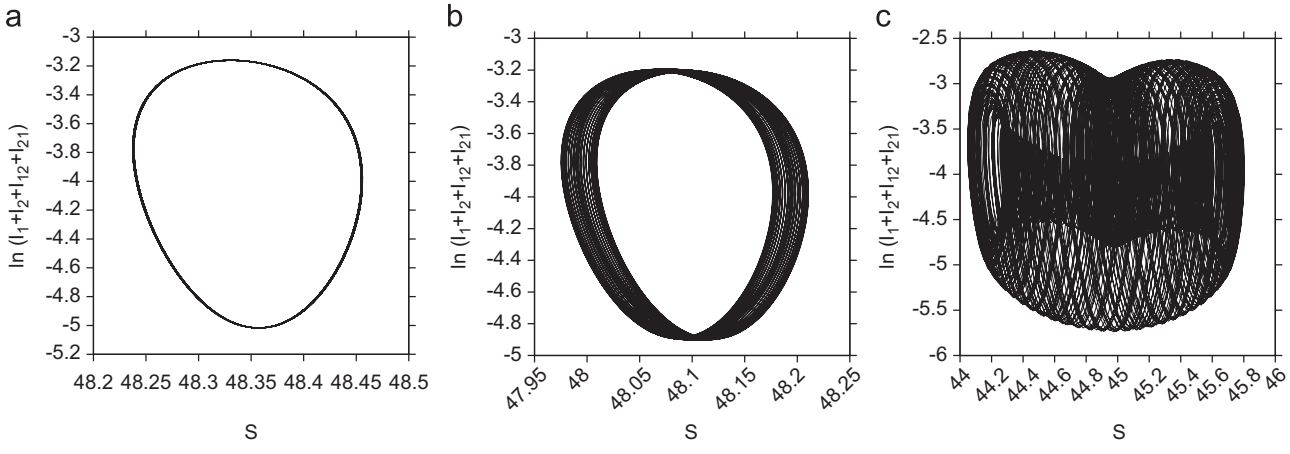

Fig. B5. Attractors in state space for the low seasonal model. Here 2000 years of transients were discarded. In (a) the period one attractor for $\phi = 0.1$, in (b) the torus attractor for $\phi = 0.114535$, the torus bifurcation point calculated by AUTO. In (c) the torus attractor for $\phi = 0.3$.

with $0 \le t \le T$ where $T = 2\pi$. This periodic solution is stable because we have $\lim_{t\to\infty} r(t) = \eta$, independent of $r_0 > 0$.

In AUTO (Doedel and Oldeman, 2009) the stability of the periodic solution $\tilde{x}(t)$,$\tilde{y}(t)$, $0 \ne t \le T$, may be analyzed within the framework of Floquet theory by calculation of the multipliers, the eigenvalues of the so-called monodromy matrix. For a detailed discussion the interested reader is referred to Kuznetsov (2004). We continue with the analysis of the so-called Poincaré map.

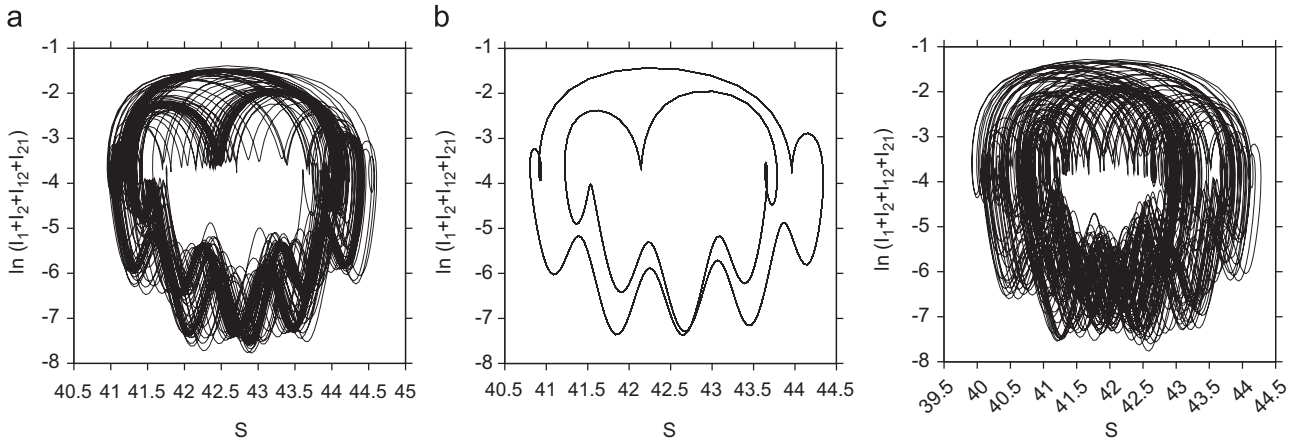

Fig. B6. Attractors in state space for the low seasonal model. Here 2000 years of transients were discarded. In (a) the attractor for $\phi = 0.431$, in (b) the period 13 attractor for $\phi = 0.44$ and in (c) the torus attractor for $\phi = 0.471$.

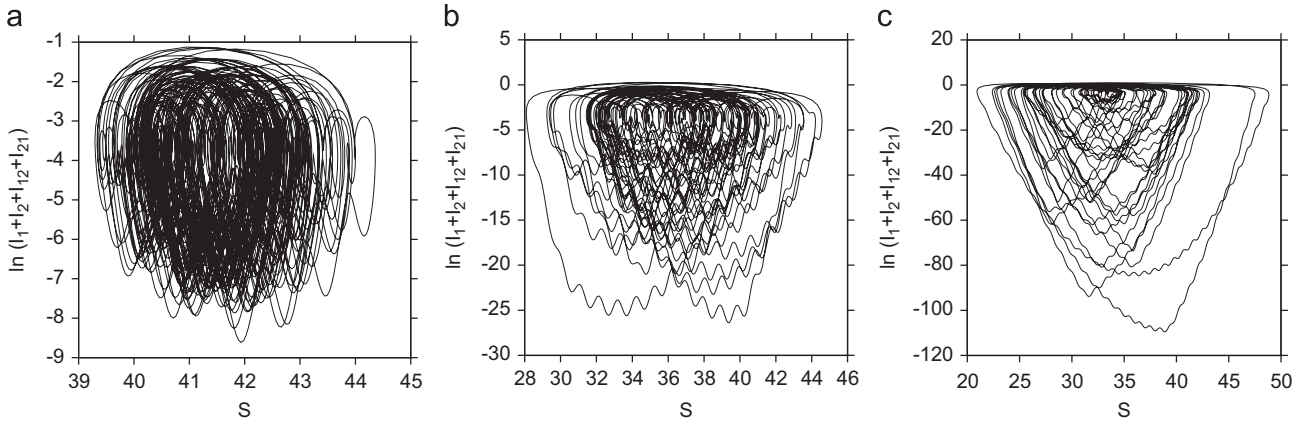

Fig. B7. Attractors in state space for the low seasonal model. Here 2000 years of transients were discarded. In (a) the chaotic attractor for $\phi = 0.5$, in (b) the chaotic attractor for $\phi = 0.8$ and in (c) the chaotic attractor for $\phi = 1$.

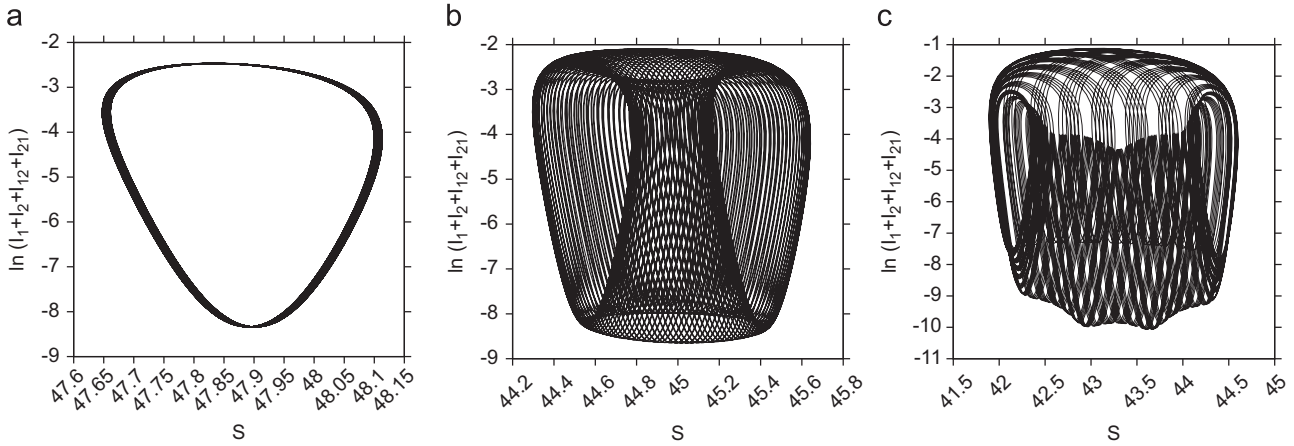

Fig. B8. Attractors in state space for the seasonal model with import of infected. Again 2000 years of transients were discarded. In (a) the torus attractor for $\phi = 0.13$, the torus bifurcation point calculated by AUTO. In (b) and in (c) the torus attractor for $\phi = 0.3$ and $\phi = 0.4$ respectively. For those ϕ values, the Lyapunov spectrum shows a slightly positive exponent indicating chaos in the torus.

Since the system is periodically forced this map is also called a stroboscopic map. The analytical expression reads

$$r_{n+1} = \eta\left(1-\left(1-\frac{\eta^2}{r_n^2}\right)e^{-4\pi\eta^2 c}\right)^{-1/2} \tag{A.10}$$

where $n \in \mathbb{N}$ and initially for $n=0$ we have $r_0 > 0$. Asymptotically we get for large n: $r_n \approx \eta$ and therefore the multiplier equals the derivative evaluated at $r = \eta$

$$\lambda = \eta e^{-4\pi\eta^2 c} \tag{A.11}$$

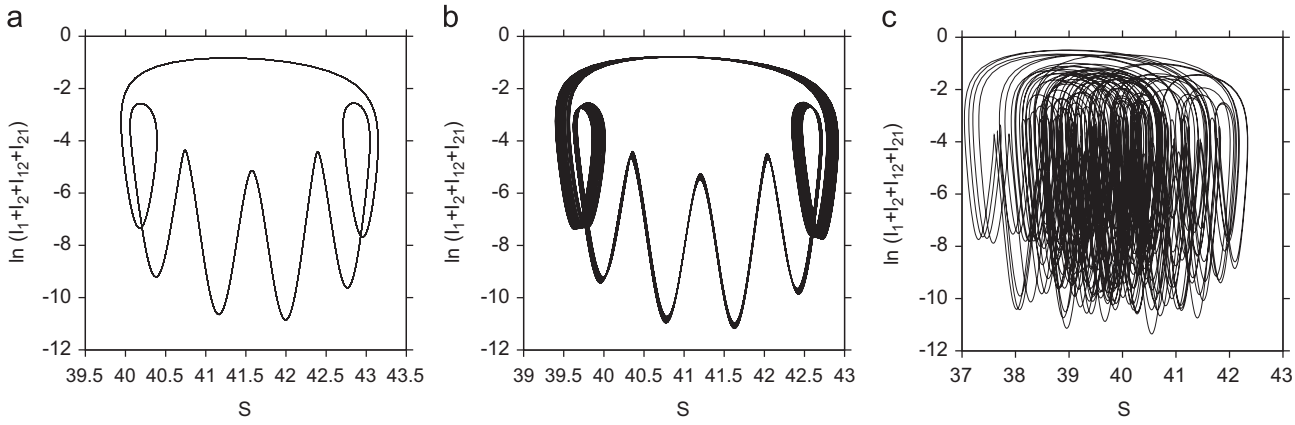

Fig. B9. Attractors in state space for the seasonal model with import of infected with 2000 years of transients discarded. In (a) the attractor for $\phi = 0.5$, in (b) torus attractor for $\phi = 0.522165$, the torus bifurcation calculated by AUTO, and in (c) the chaotic attractor found in the region of ϕ between 0.5 and 1. Here for $\phi = 0.6$.

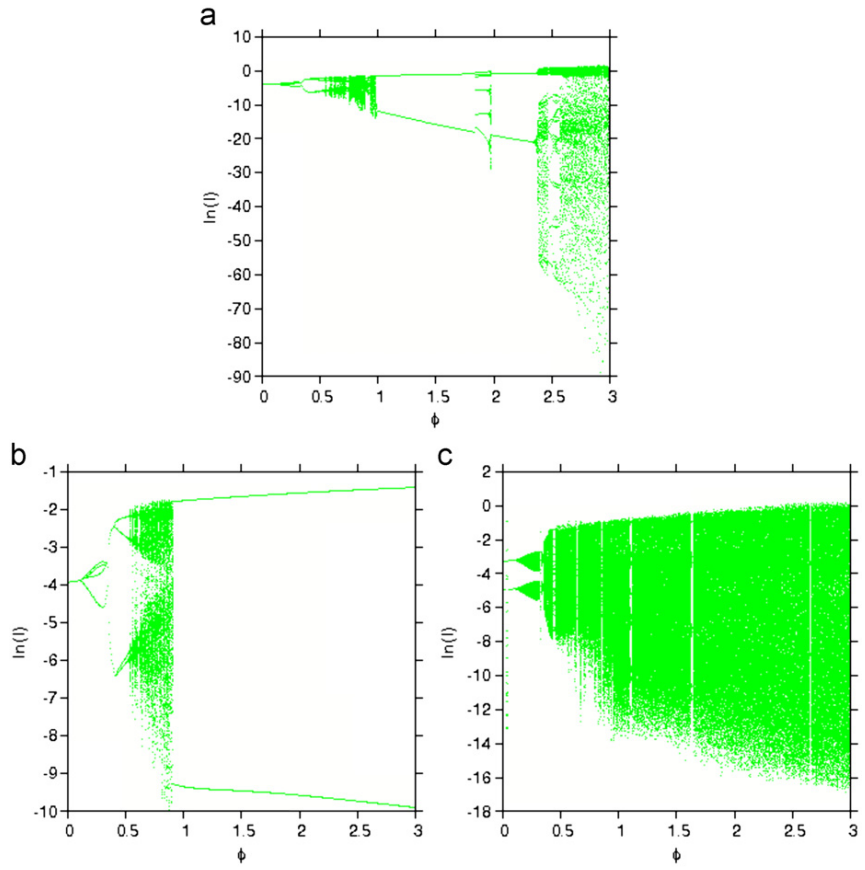

Fig. C1. Bifurcation diagram comparison between the non-seasonal model, the non-seasonal model with import and the low seasonal model with import. In (a) we show the bifurcation diagram for the original non-seasonal model previously studied in Aguiar and Stollenwerk (2007) and Aguiar et al. (2008, 2009), where two chaotic windows were found. A new chaotic window in a ϕ region where the ratio of secondary infection contribution to the force of infection is smaller than 1 and also the classical chaotic window found previously in Ferguson et al. (1999) and Aguiar et al. (2008), where the ratio of secondary infection contribution to the force of infection is much larger than 1, actually ≈ 3. In (b) we show the bifurcation diagram for the non-seasonal model described in Aguiar et al. (2008) with addition of a low import of infected. Here we see that the import removes the complex dynamics in the region of ϕ larger than 1 where the stable limit cycle (crossing the right boundary of Fig. 2b) is the unique attractor. In (c) we show the bifurcation diagram for the extended multi-strain model, the low seasonal model with import, where the chaotic attractors are back for even larger parameter regions.

This single multiplier is less than 1 and therefore the periodic solution is stable.

Since this Hopf-system is decoupled from the system (1) and therefore the Lyapunov exponents of the augmented system are those of the original system (1) together with zero (Haken, 1983) and expression (A.11). For the Lyapunov spectrum of the seasonal dengue models with parameter ϕ between $\phi = 0$ and $\phi = 1.2$, we plot the first six exponents coupled with the Hopf oscillator

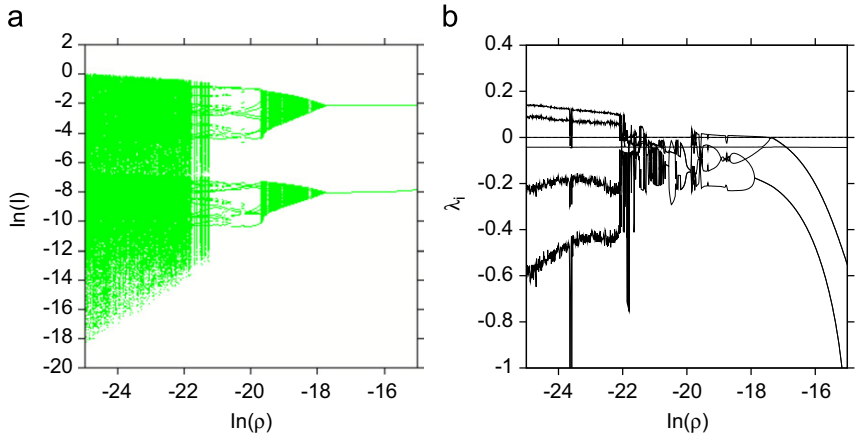

Fig. D1. Bifurcation diagram for the import parameter and its Lyapunov spectrum. Here we vary the import factor ρ (in log scale). The other parameters are fixed as it follows: temporary cross-immunity $\alpha = 2$, recovery rate $\gamma = 52\ y^{-1}$, secondary infection contribution to the force of infection $\phi = 0.9$, the infection rate $\beta_0 = 2 \cdot \gamma$, degree of seasonality $\eta = 0.35$, and birth and death rate $\mu = 1/65$ y.

where the parameters are $\eta = 0.1$, $\omega = 2 \cdot \pi$ and contraction rate $c = 5000$, hence from the Hopf oscillator the Lyapunov exponent are $\lambda_1 = -2c\eta^2 = -100$ and $\lambda_2 = 0$.

Appendix B. Attractors in state space

In this section we show the transitions between different attractors in state space plot for the three studied scenarios, the non-seasonal model (see Appendix B.1), the low seasonal model (see Appendix B.2) and the seasonal model with import of infected (see Appendix B.3). The parameters are given in Table 1.

B.1. Attractors in state space for the non-seasonal multi-strain dengue model

Figs. B1–B3 show the attractors in state space plot for the non-seasonal model.

B.2. Attractors in state space for the low seasonal multi-strain dengue model

Figs. B4–B6 show the attractors in state space plot for the low seasonal model.

B.3. Attractors in state space for the seasonal multi-strain dengue model with import of infected

Figs. B7 and B8 show the attractors in state space plot for the seasonal model with import of infected.

Appendix C. The non-seasonal model with low import factor versus the low seasonal model with low import factor

In this section we show the bifurcation diagram comparison between the original non-seasonal model, the non-seasonal model with import and the low seasonal model with import. The addition of a low import factor into the original non-seasonal system gives a stable limit cycle as the unique attractor (see Fig. C1(b)), in contrast with the results for the original non-seasonal models analyzed in Ferguson et al. (1999) and Aguiar et al. (2008, 2009), where two chaotic windows were found (see Fig. C1(a)). Adding low seasonality to this system brings the chaotic attractors back for even larger parameter regions (see Fig. C1(c)). These results are important since we expect complex dynamics to explain the fluctuations observed in empirical data, when the ratio of secondary infection contribution to the force of infection could be slightly smaller or larger than 1, not needing to restrict the ADE effect to one or another region in parameter space.

Appendix D. Lyapunov exponents and import factor

In this section we extend the analysis of the seasonal model with import with a bifurcation analysis where the import ρ is varying. The Lyapunov spectrum together with the bifurcation diagram confirm the importance of adding import into the dynamical model. An import factor $\ln(\rho) = -18$ or less leads to complex behavior while with a very high import factor of infected periodic solutions are observed. The understanding of such complex scenario opens possibilities to analyze the available data.

References

Aguiar, M., Stollenwerk, N., 2007. A new chaotic attractor in a basic multi-strain epidemiological model with temporary cross-immunity. arXiv:0704.3174v1 [nlin.CD].

Aguiar, M., Kooi, B.W., Stollenwerk, N., 2008. Epidemiology of dengue fever: a model with temporary cross-immunity and possible secondary infection shows bifurcations and chaotic behaviour in wide parameter regions. Math. Model. Nat. Phenom. 4, 48–70.

Aguiar, M., Stollenwerk, N., Kooi, B.W., 2009. Torus bifurcations, isolas and chaotic attractors in a simple dengue model with ADE and temporary cross immunity. Int. J. Comput. Math. 86, 1867–1877.

Aguiar, M., Ballesteros, S., Boto, J.P., Kooi, B.W., Mateus, L., Stollenwerk, N. Parameter estimation in epidemiology: from simple to complex dynamics. AIP Conference Proceedings ICNAAM 2011, Greece, accepted for publication.

Alcon, S., et al., 2002. Enzyme-linked immunosorbent assay specific to Dengue Virus Type 1 nonstructural protein NS1 reveals circulation of the antigen in the blood during the acute phase of disease in patients experiencing primary or secondary infections. J. Clin. Microbiol. 40, 376–381.

Billings, L., et al., 2007. Instabilities in multiserotype disease models with antibody-dependent enhancement. J. Theor. Biol. 246, 18–27.

Chareonsook, O., Foy, H.M., Teeraratkul, A., Silarug, N., 1999. Changing epidemiology of dengue hemorrhagic fever in Thailand. Epidemiol. Infect. 122, 161–166.

David, W.V., 2000. Invited commentary: dengue lessons from Cuba. Am. J. Epidemiol. 152, 800–803.

Dejnirattisai, W., et al., 2010. Cross-reacting antibodies enhance dengue virus infection in humans. Science 328, 745–748.

Diniz, S., Fundao Ezequiel Dias, Minas Gerais, Brazil.

Doedel, J.E., Oldeman, B., 2009. AUTO 07P Continuation and Bifurcation Software for Ordinary Differential Equations. Technical Report. Concordia University, Montreal, Canada, Retrieved from ⟨http://indy.cs.concordia.ca/auto/⟩.

Eckmann, J.-P., Kamphorst, O.S., Ruelle, D., Cilliberto, S., 1986. Liapunov exponents from time series. Phys. Rev. A 34, 4971–4979.
Endy, T.P., et al., 2002. Spatial and temporal circulation of dengue virus serotypes: a prospective study of primary school children in Kamphaeng Phet, Thailand. Am. J. Epidemiol. 156, 52–59.
Esteva, L., Vargas, C., 1998. Analysis of a dengue disease transmission model. Math. Biosci. 150, 131–151.
Esteva, L., Vargas, C., 2000. Influence of vertical and mechanical transmission on the dynamics of dengue disease. Math. Biosci. 167, 51–64.
Ferguson, N., Anderson, R., Gupta, S., 1999. The effect of antibody-dependent enhancement on the transmission dynamics and persistence of multiple-strain pathogens. Proc. Natl. Acad. Sci. USA 96, 790–794.
Fischer, D.B., Halstead, S.B., 1970. Observations related to pathogenesis of dengue hemorrhagic fever. V. Examination of age specific sequential infection rates using a mathematical model. J. Biol. Med. 42, 329–349.
Gibbons, V.R., et al., 2007. Analysis of repeat hospital admissions for dengue to estimate the frequency of third or fourth dengue infections resulting in admissions and dengue hemorrhagic fever, and serotype sequences. Am. J. Trop. Med. Hyg. 77, 910–913.
Gubler, J.D., Suharyono, W., Tan, R., Abidin, M., Sie, A., 1981. Viraemia in patients with naturally acquired dengue infection. Bull WHO 59, 623–630.
Guckenheimer, J., Holmes, P., 1985. Nonlinear oscillations, dynamical systems and bifurcations of vector fields. In: Applied Mathematical Sciences, vol. 42, 2nd ed. Springer-Verlag, New York.
Guzmán, M.G., et al., 2000. Epidemiologic studies on dengue in Santiago de Cuba, 1997. Am. J. Epidemiol. 152, 793–799.
Haken, H., 1983. At least one Lyapunov exponent vanishes if the trajectory of an attractor does not contain a fixed point. Phys. Lett. 94A, 71–72.
Halstead, S.B., 1982. Immune enhancement of viral infection. Progr. Allergy 31, 301–364.
Halstead, S.B., 2003. Neutralization and antibody-dependent enhancement of dengue viruses. Adv. Virus Res. 60, 421–467.
Halstead, S.B., 2004. Antibody-dependent enhancement of infection: a mechanism for indirect virus entry into cells. Cellular Receptor for Animal Viruses, vol. 28. Cold Spring Harbor Laboratory Press, pp. 493–516 0-87969-429-7/94 (Chapter 25).
Halstead, S.B. (Ed.), 2008. Tropical Medicine: Science and Practice. Dengue, vol. 5. Imperial College Press (Chapter 7).
Halstead, S., Pedriatic Dengue Vaccine Initiative, MD, USA.
He, D., Ionides, E.L., King, A.A., 2010. Plug-and-play inference for disease dynamics: measles in large and small populations as a case study. J. R. Soc. Interface 7, 271–283.
Holzfuss, J., Lauterborn, W., 1989. Liapunov exponents from a time series of acoustic chaos. Phys. Rev. A 39, 2146–2152.
Holzfuss, J., Parlitz, U., 1991. Lyapunov exponents from time series. Lecture Notes in Mathematics, vol. 1486; 1991, pp. 263–270.
Ionides, E., Breto, C., King, A.A., 2006. Inference for nonlinear dynamical systems. Proc. Natl. Acad. Sci. USA 103, 18438–18443.
Kooi, B.W.v., Voorn, A.K.G., pada Das, K., 2011. Stabilisation and complex dynamics in a predator–prey model with predator suffering from an infectious disease. Ecol. Complexity 8, 113–122.
Kuznetsov, Y.A., 2004. Elements of applied bifurcation theory. In: Mathematical Sciences, vol. 112, 3rd ed. Springer-Verlag, New York.
Lemos, F., Pers comm. Secretaria de Estado de Saúde de Minas Gerais, Brazil.
Malchow, H., Petrovskii, S.V., Venturino, E., 2008. Spatiotemporal patterns in ecology and epidemiology: theory, models, and simulation. In: Mathematical & Computational BiologyChapman & Hall, CRC Press.
Matheus, S., et al., 2005. Discrimination between primary and secondary dengue virus infection by an immunoglobulin G avidity test using a single acute-phase serum sample. J. Clin. Microbiol. 43, 2793–2797.
Nagao, Y., Koelle, K., 2008. Decreases in dengue transmission may act to increase the incidence of dengue hemorrhagic fever. Proc. Natl. Acad. Sci. USA 105, 2238–2243.
Nisalak, A., et al., 2003. Serotype-specific dengue virus circulation and dengue disease in Bangkok, Thailand from 1973 to 1999. Am. J. Trop. Med. Hyg. 68, 191–202.
Ott, E., 1993. Chaos in Dynamical Systems, 2nd ed. Cambridge University Press, Cambridge.
Pediatric Dengue Vaccine Initiative. International Vaccine Institute (IVI). Global Burden of Dengue. Retrieved from 〈http://www.pdvi.org/about_dengue/GBD.asp〉.
Recker, M., et al., 2009. Immunological serotype interactions and their effect on the epidemiological pattern of dengue. Proc. R. Soc. B 276, 2541–2548.
Rothman, A.L., 2004. Dengue: defining protective versus pathologic immunity. J. Clin. Invest. 113, 946–951.
Schwartz, I.B., Shaw, L.B., Cummings, D.A.T., Billings, L., McCrary, M., Burke, D.S., 2005. Chaotic desynchronization of multi-strain diseases. Phys. Rev. E 72, 066201–066206.
Stiefs, D., Venturino, E., Feudel, U., 2009. Evidence of chaos in eco-epidemic models. Math. Biosci. Eng. 6, 855–871.
Stollenwerk, N., Jansen, V.A.A., 2003. Meningitis, pathogenicity near criticality: the epidemiology of meningococcal disease as a model for accidental pathogens. J. Theor. Biol. 222, 347–359.
Stollenwerk, N., Maiden, M.C.J., Jansen, V.A.A., 2004. Diversity in pathogenicity can cause outbreaks of menigococcal disease. Proc. Natl. Acad. Sci. USA 101, 10229–10234.
Stone, L., Olinky, R., Huppert, A., 2007. Seasonal dynamics of recurrent epidemics. Nature 446, 533–536.
Wearing, H.J., Rohani, P., 2006. Ecological and immunological determinants of dengue epidemics. Proc. Natl. Acad. Sci. USA 103, 11802–11807.
Wikipedia contributors. Wikipedia, The Free Encyclopedia. Provinces of Thailand. Retrieved from 〈http://en.wikipedia.org/wiki/Provinces_of_Thailand〉.
Wikramaratna, P.S., et al., 2010. The effects of tertiary and quaternary infections on the epidemiology of dengue. PLoS ONE 5, e12347.
World Health Organization, 2009. Dengue and Dengue Hemorrhagic Fever Fact sheet 117. Retrieved from 〈http://www.who.int/mediacentre/factsheets/fs117/en/〉.
World Population Prospects. The 2008. Revision Population Database. Retrieved from 〈http://esa.un.org/unpp/index.asp?panel=2〉.